International Forum on Aeroelasticity and Structural Dynamics
IFASD 2017
25-28 June 2017 Como, Italy

AEROM: NASA'S UNSTEADY AERODYNAMIC AND AEROELASTIC REDUCED-ORDER MODELING SOFTWARE

Walter A. Silva*
NASA Langley Research Center, Hampton, Virginia
[1]

Abstract:

The origins, development, implementation, and application of AEROM, NASA's patented reduced-order modeling (ROM) software, are presented. Full computational fluid dynamic (CFD) aeroelastic solutions and ROM aeroelastic solutions, computed at several Mach numbers using the NASA FUN3D CFD code, are presented in the form of root locus plots in order to better reveal the aeroelastic root migrations with increasing dynamic pressure. The method and software have been applied successfully to several configurations including the Lockheed-Martin N+2 supersonic configuration and the Royal Institute of Technology (KTH, Sweden) generic wind-tunnel model, among others. The software has been released to various organizations with applications that include CFD-based aeroelastic analyses and the rapid modeling of high-fidelity dynamic stability derivatives. Recent results obtained from the application of the method to the AGARD 445.6 wing will be presented that reveal several interesting insights.

1 INTRODUCTION

Classical linear aeroelastic analyses typically produce Velocity-damping-frequency (V-g-f) plots and/or root locus plots. The use of these plots has enabled aeroelasticians to view the nature of the flutter mechanisms in addition to identifying the conditions at which flutter occurs. The rapid creation of these plots was facilitated by the use of linear unsteady aerodynamics and linear aeroelastic equations of motion [1].

During the last few years, higher-order Computational Fluid Dynamics (CFD)-based methods have become an important tool for the computation of nonlinear unsteady aerodynamics for use in aeroelastic analyses. The use of these higher-order tools provides valuable insight regarding complex flow physics at conditions where linear methods are not theoretically valid. However, the increased computational cost associated with the computation of unsteady aerodynamics and aeroelastic responses using higher-order methods has resulted in a subtle change in the manner in which the aeroelastician evaluates and interprets these analyses. First, the increased computational cost of these analyses has tended to dictate a snapshot approach to aeroelastic analyses whereby the aeroelastic response at only a handful of dynamic pressures is all that is computed. This snapshot approach is used to identify the flutter dynamic pressure but the actual flutter mechanism is not easily discernible. Second, due to the complexity of the computational analyses, methods that could rapidly generate V-g-f plots and/or root locus plots are not available. However, with the development of reduced-order modeling (ROM) methods [2–4], the rapid generation of root locus plots using CFD-based unsteady aerodynamics is now available to aeroelasticians.

*Senior Research Scientist, Aeroelasticity Branch, AIAA Associate Fellow.

The origin of this method started with the author's PhD dissertation [5] and related publications [6, 7]. An important conceptual development first presented in these references consists of the realization that unsteady aerodynamic impulse responses exist and can be computed. This concept is an important point that is claimed to be not realizable in some of the classic aeroelastic references. The reason for this discrepancy is actually quite simple as it relates to the difference between the impulse function for a continuous-time system versus that for a discrete-time system.

For a continuous-time system, it is well known that the impulse input function is the Dirac delta function. This function serves the continuous domain well, in particular in the solution of ordinary and partial differential equations. However, its application to a discrete-time system such as a CFD-based solution, is not clear, thus the belief that an impulse input could not be applied to a CFD code. Therefore, if an impulse input could not be applied to a CFD code, then an unsteady aerodynamic response could not be identified or realized.

An important contribution by the author [5] is the realization that in order to properly identify the unsteady aerodynamic impulse response using a CFD code, a discrete-time impulse input, also known as the unit sample input in discrete-time theory, is the proper function to use and not the Dirac delta function. The theory of Digital Signal Processing (DSP) demonstrates that a unit sample input is much simpler to apply and less complex to interpret than the Dirac delta function. These results proved the existence and realizability of a unit unsteady aerodynamic impulse (sample) response via a CFD code.

In the world of structural dynamics and modal identification, the concept of a structural dynamic impulse response is clear and well understood. As a result, various modal identification techniques consist of the identification of these responses and a subsequent realization of a system that captures the structural dynamic system of interest. Having familiarity with one of these methods by the name of Eigensystem Realization Algorithm (ERA) [8]/System Observer Controller Identification Toolbox (SOCIT) [9], the author applied the modal identification technique, previously limited to structural dynamic systems, to that of identifying an unsteady aerodynamic system via the identification of the unsteady aerodynamic impulse responses. Once the concept of a discrete-time unsteady aerodynamic impulse response was mathematically validated, the application of ERA/SOCIT became quite logical [10]. These results [10] represent the first time that the ERA/SOCIT algorithms were used for the identification of unsteady aerodynamic systems. It is valuable to point out that this method is now being applied at several organizations around the world [11–16]. In the area of fluid modal decompositions using, primarily, the Proper Orthogonal Decomposition (POD), the application of the ERA algorithm has become standard, with an initial appearence in the literature by Ma, Ahuja, and Rowley [17].

Following these fundamental advances, Silva and Bartels [18] introduced the development of linearized, unsteady aerodynamic state-space models for prediction of flutter and aeroelastic response using the parallelized, aeroelastic capability of the CFL3Dv6 code. The results presented provided an important validation of the various phases of the ROM development process. The ERA, which transforms an impulse response (one form of a ROM) into state-space form (another form of a ROM), was applied to the development of the aerodynamic state-space models. Flutter results for the AGARD 445.6 aeroelastic wing were calculated using the CFL3Dv6 code, including computational costs [18]. Unsteady aerodynamic state-space models were generated and coupled with a structural model within a MATLAB/SIMULINK^{TM} environment for rapid calculation of aeroelastic responses including the prediction of flutter. Aeroelastic responses

computed directly using the aeroelastic simulation ROM showed excellent comparison with the aeroelastic responses computed using the CFL3Dv6 code [19].

Previously [18], the aerodynamic impulse responses (unit pulses) that were used to generate the unsteady aerodynamic state-space model were computed via the excitation of one mode at a time. For a four-mode system such as the AGARD 445.6 wing, these computations are not very expensive. However, for more realistic cases where the number of modes can be an order of magnitude or more larger, the one-mode-at-a-time method becomes prohibitively expensive, requiring a different approach. Kim et al [20] have proposed methods that enable the simultaneous application of structural modes as CFD input, greatly reducing the cost of identifying the aerodynamic impulse responses from the CFD code. Kim's method consists of using simultaneous staggered step inputs, one per mode, and then recovering the individual responses from this simultaneous excitation. Silva [2] has developed a method that enables the simultaneous excitation of the structural modes using orthogonal functions. Both of these methods require only a single CFD solution and the methods are independent of the number of structural modes.

Silva [21] has also developed a method for generating static aeroelastic solutions and matched-point aeroelastic solutions using a ROM. The methods developed by Silva [2, 21] have already been implemented in the FUN3D [22–25] CFD code. In addition, methods for generating root locus plots of the combined structural state-space model and unsteady aerodynamic state-space model were developed by Silva et al [3]. These ROM-based root locus methods were applied to fixed-wing configurations and subsequently to launch vehicle configurations [4]. The present paper will discuss the application of these ROM and root locus methods in order to visualize the aeroelastic behavior of the various aerospace configurations.

In November 2011, the AEROM software was granted a patent, Patent No. 8,060,350. The software has been distributed to the Air Force Research Laboratory, the Boeing Corporation, and the CFD Research Corporation.

2 COMPUTATIONAL METHODS

2.1 FUN3D Code

The unstructured mesh solver used for this study is FUN3D. Within the code, the unsteady Navier-Stokes equations are discretized over the median dual volume surrounding each mesh point, balancing the time rate of change of the averaged conserved variables in each dual volume with the flux of mass, momentum and energy through the instantaneous surface of the control volume.

Because the CFD and computational structural mechanics (CSM) meshes usually do not match at the boundary interface where the grids are defined, CFD/CSM coupling requires a surface spline interpolation between the two domains. The interpolation of CSM mode shapes to CFD surface grid points is done as a preprocessing step [26]. Modal deflections at the CFD surface grids are first generated. Mode shape displacements located at CFD surface grid points are used in the integration of the generalized modal forces and in the computation of the deflection of the deformed surface. The final surface deformation at each time step is a linear superposition of all the modal deflections.

2.2 System Identification Method

In structural dynamics, the realization of discrete-time state-space models that describe the modal dynamics of a structure has been enabled by the development of algorithms such as the ERA [8] and the Observer Kalman Identification (OKID) [27] Algorithm. These algorithms perform state-space realizations by using the Markov parameters (discrete-time impulse responses) of the systems of interest. These algorithms have been combined into one package known as SOCIT developed at NASA Langley Research Center.

There are several algorithms within the SOCIT that are used for the development of unsteady aerodynamic discrete-time state-space models. The PULSE algorithm is used to extract individual input/output impulse responses from simultaneous input/output responses. For a four-input/four-output system, simultaneous excitation of all four inputs yields four output responses. The PULSE algorithm is used to extract the individual sixteen (all combinations of four inputs and four outputs) impulse responses that associate the response in each of the outputs due to each of the inputs. Once the individual sixteen impulse responses are available, they are then processed via the ERA in order to transform the sixteen individual impulse responses into a four-input/four-output, discrete-time, state-space model. A brief summary of the basis of this algorithm follows.

A finite dimensional, discrete-time, linear, time-invariant dynamical system has the state-variable equations

$$x(k+1) = Ax(k) + Bu(k) \tag{1}$$

$$y(k) = Cx(k) + Du(k) \tag{2}$$

where *x* is an n-dimensional state vector, *u* an m-dimensional control input, and *y* a p-dimensional output or measurement vector with *k* being the discrete time index. The transition matrix, *A*, characterizes the dynamics of the system. The goal of system realization is to generate constant matrices (*A, B, C, D*) such that the output responses of a given system due to a particular set of inputs is reproduced by the discrete-time state-space system described above.

For the system of Eqs. (1) and (2), the time-domain values of the discrete-time impulse responses of the system are also known as the Markov parameters and are defined as

$$Y(k) = CA^{k-1}B + D \tag{3}$$

with *A* an (n x n) matrix, *B* an (n x m) matrix, *C* a (p x n) matrix, and *D* an (p x m) matrix. The ERA algorithm begins by defining the generalized Hankel matrix consisting of the discrete-time impulse responses for all input/output combinations. The algorithm then uses the singular value decomposition to compute the (*A, B, C, D*) matrices.

In this fashion, the ERA is applied to unsteady aerodynamic impulse responses to construct unsteady aerodynamic state-space models.

2.3 Simultaneous Excitation Input Functions

Clearly, the nonlinear unsteady aerodynamic responses of a flexible vehicle comprise a multi-input/multi-output (MIMO) system with respect to the modal inputs and generalized aerodynamic outputs. In the situation where the goal is the simultaneous excitation of such a MIMO system, system identification techniques [28–30] dictate that the nature of the input functions

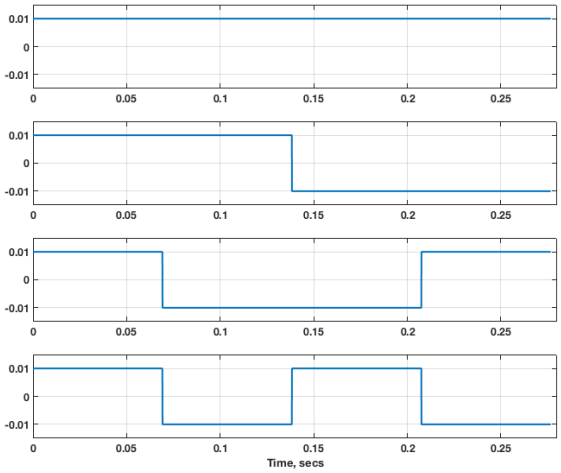

Figure 1: Walsh functions.

used to excite the system must be properly defined if accurate input/output models of the system are to be generated. The most important point to keep in mind when defining these input functions is that these functions need to be different, in some sense, from each other. If the excitation inputs are identical, for example, and are applied simultaneously, it is quite difficult to separate the effects of one input from the others. This, in turn, makes it practically impossible for a system identification algorithm to extract the individual impulse responses for each input/output pair. As has already been well established, the individual impulse responses for each input/output pair are necessary ingredients towards the development of state-space models.

With respect to unsteady aerodynamic MIMO systems, these individual impulse responses correspond to time-domain generalized aerodynamic forces (GAFs), critical to understanding unsteady aerodynamic behavior. The Fourier-transformed version of these GAFs are the frequency-domain GAFs which provide an important link to more traditional frequency-domain-based unsteady aerodynamic analyses.

Referring back to the input functions used to excite the MIMO system, the question is how different should these input functions be from each other and how can we quantify a level of difference between them? Since orthogonality (linear independence) is the most precise mathematical method for guaranteeing the difference between signals, recent developments focused on the application of families of orthogonal functions as candidate input functions. Using orthogonal functions directly provides a mathematical guarantee that the input functions are as different from each other as mathematically possible. These orthogonal input functions can be considered optimal input functions for the identification of a MIMO system.

In a previous paper [2], four families of functions were investigated to efficiently identify a CFD-based unsteady aerodynamic state-space model. For the present paper, the Walsh family of orthogonal functions [31] are used, shown in Figure 1 for four modes. These functions are orthogonal and therefore provide a benefit in the system identification process as discussed above. Also, this family of functions consists of a combination of step functions, which have been shown to be well-suited for the identification of CFD-based unsteady aerodynamic ROMs.

3 ROM DEVELOPMENT PROCESSES

The ROM development process consists of two parts: the creation of the unsteady aerodynamic ROM and the creation of the structural dynamic ROM. The combination of the unsteady aerodynamic ROM with the structural dynamic ROM yields what is referred to as the aeroelastic simulation ROM.

The original unsteady aerodynamic ROM development process consisted of the excitation of one structural mode at a time per CFD solution. That approach is not practical for realistic configurations with a large number of modes. As mentioned above, an improved method has been developed and is described below.

3.1 Improved ROM Development Process

An outline of the improved simultaneous modal excitation ROM development process is as follows:

1. Generate the number of functions (from a selected family of orthogonal functions) that corresponds to the number of structural modes;
2. Apply the generated input functions simultaneously via one CFD execution resulting in GAF responses due to these inputs; these responses are computed directly from the restart of a steady rigid CFD solution (not about a particular dynamic pressure);
3. Using the simultaneous input/output responses, identify the individual impulse responses using the PULSE algorithm (within SOCIT);
4. Transform the individual impulse responses generated in Step 3 into an unsteady aerodynamic state-space system using the ERA (within SOCIT);
5. Evaluate/validate the state-space models generated in Step 4 via comparison with CFD results (i.e., ROM results vs. full CFD solution results);

A schematic of steps 1-4 of the improved process outlined above is presented as Figure 2.

Using modal information (generalized masses, modal frequencies, and modal dampings), a state-space model of the structure is generated. This state-space model of the structure is referred to as the structural dynamic ROM (Figure 3). Once an unsteady aerodynamic ROM and a structural dynamic ROM have been generated, they are combined to form an aeroelastic simulation ROM (see Figure 4). Then root locus plots are extracted from the aeroelastic simulation ROM.

An important difference between the original ROM process and the improved ROM process is stated in step (2) of the outline above. For the original ROM process, if a static aeroelastic condition existed, then a ROM was generated about that selected static aeroelastic condition. So a static aeroelastic condition of interest would be defined (typically based on a dynamic pressure) and that static aeroelastic condition was generated using the CFD code as a restart from a converged steady, rigid solution. Once a converged static aeroelastic solution was obtained, the development of the unsteady aerodynamic ROM process was applied about that static aeroelastic condition. This approach implies that the resultant unsteady aerodynamic ROM is limited in some sense to the neighborhood of that static aeroelastic condition. Moving too far away from that condition could result in loss of accuracy.

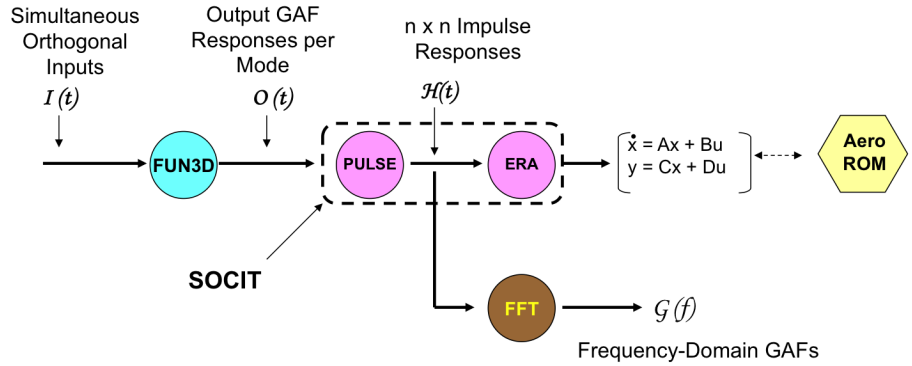

Figure 2: Improved process for generation of an unsteady aerodynamic ROM (Steps 1-4).

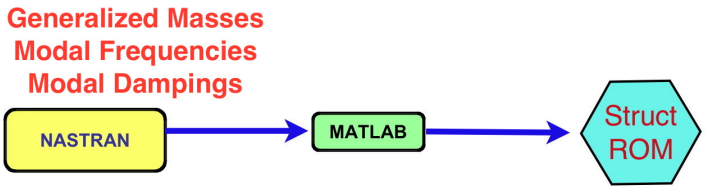

Figure 3: Process for generation of a structural state-space ROM.

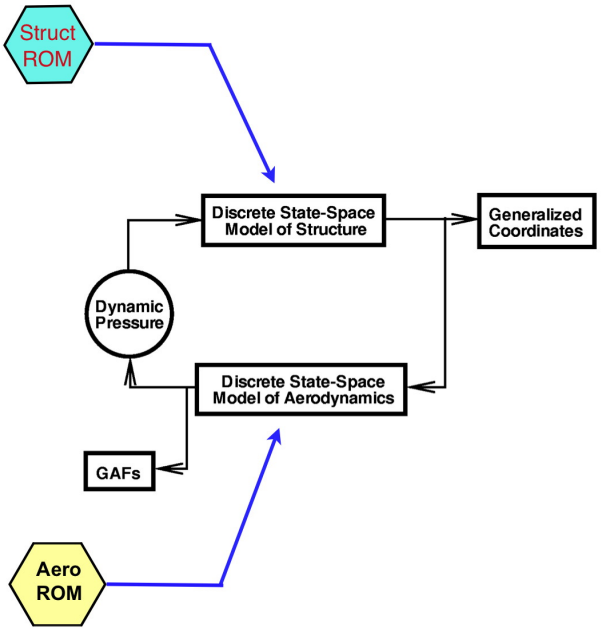

Figure 4: Process for generation of an aeroelastic simulation ROM consisting of an unsteady aerodynamic ROM and a structural state-space ROM.

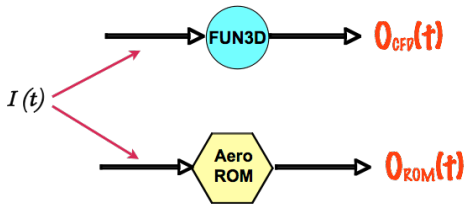

Figure 5: Error defined as difference between the FUN3D solution and the unsteady aerodynamic ROM solution due to input of orthogonal functions.

The reason ROMs were generated in this fashion was because no method had been defined to enable the computation of a static aeroelastic solution using a ROM. Any ROMs generated in this fashion were, therefore, limited to the prediction of dynamic responses about a static aeroelastic solution including the methods by Raveh [32] and by Kim et al [20]. The improved ROM method, however, includes a method for generating a ROM directly from a steady, rigid solution. As a result, these improved ROMs can then be used to predict both static aeroelastic and dynamic solutions for any dynamic pressure. In order to capture a specific range of aeroelastic effects (previously obtained by selecting a particular dynamic pressure), the improved ROM method relies on the excitation amplitude of the orthogonal functions to excite aeroelastic effects of interest. The details of the method for using a ROM for computing both static aeroelastic and dynamic solutions is presented in another reference by the author [21]. For the present results, all responses were computed from the restart of a steady, rigid FUN3D solution, bypassing the need (and the additional computational expense) to execute a static aeroelastic solution using FUN3D.

3.2 Error Minimization

Error minimization consists of error quantification and error reduction. Error quantification is defined as the difference (error) between the full FUN3D solution due to the orthogonal input functions used (Walsh) and the unsteady aerodynamic ROM solution due to the same orthogonal input functions. This was identified in Step 5 in the previous subsection and is shown schematically in Figure 5. The outputs shown are GAF responses per mode. Within the system identification algorithms, there are parameters that can then be used to reduce the error (error reduction). These parameters include number of states and the record length of the identified pulse responses, for example. The maximum error is the largest error encountered per mode. Using the maximum error as the figure of merit, the parameters are varied until an acceptable ROM has been obtained.

4 SAMPLE RESULTS

A brief summary of results for three configurations is presented in this section. These configurations are the Lockheed-Martin N+2 low-boom supersonic configuration, the Royal Institute

of Technology (KTH) generic fighter wind-tunnel model, and the AGARD 445.6 wing.

4.1 Low-Boom N+2 Configuration

An artist's rendering of the Lockheed-Martin N+2 low-boom supersonic configuration is presented in Figure 6. This configuration has been used extensively as part of a NASA research effort to address the technologies required for a low-boom aircraft, including aeroelastic effects. Presented in Figure 7 is a comparison of the dynamic aeroelastic responses of the time histories of the fourth mode generalized displacements from a full FUN3D aeroelastic solution and the ROM aeroelastic solution at a dynamic pressure of 2.149 psi for the N+2 low-boom configuration. As can be seen, the results are practically identical. Similar results are obtained for all the other modes, indicating good confidence in the ROM.

Figure 6: Artist's concept of the Lockheed-Martin N+2 configuration.

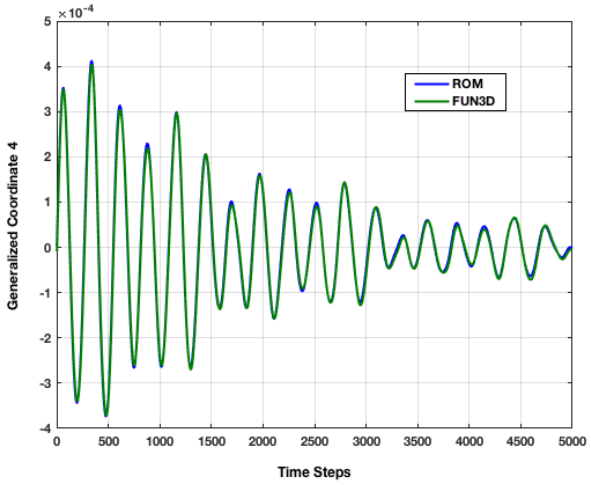

Figure 7: Comparison of full FUN3D aeroelastic response and ROM aeroelastic response for the fourth mode of the N+2 configuration at M=1.7 and a dynamic pressure of 2.149 psi.

A major benefit of this ROM technology is the ability to rapidly generate an aeroelastic root locus plot that reveals the aeroelastic mechanisms occurring at that flight condition. Figure 8 presents the aeroelastic root locus plot for the low-boom N+2 configuration at M=1.70. This root locus plot clearly indicates the aeroelastic mechanisms that affect this configuration. In the root locus plot, each symbol represents the aeroelastic roots at a specific dynamic pressure. In

this case, each increment in dynamic pressure corresponds to 2 psi. It is important to mention that this root locus plot is generated in seconds while multiple full FUN3D solutions would be required for each dynamic pressure of interest, with each solution requiring about two days.

The computational cost of generating these ROM solutions consists of one full FUN3D solution that is used to generate the ROM at that Mach number. This full FUN3D solution ran for three hours and consisted of 2400 time steps. Once this solution is available, a ROM can be generated and then used to generate all the aeroelastic responses at all dynamic pressures. In comparison, a full FUN3D analysis at each dynamic pressure requires two full FUN3D solutions: a static aeroelastic (10 hours) and a dynamic aeroelastic (18 hours). Therefore, full FUN3D solutions for 20 dynamic pressures would require 560 hours of compute time.

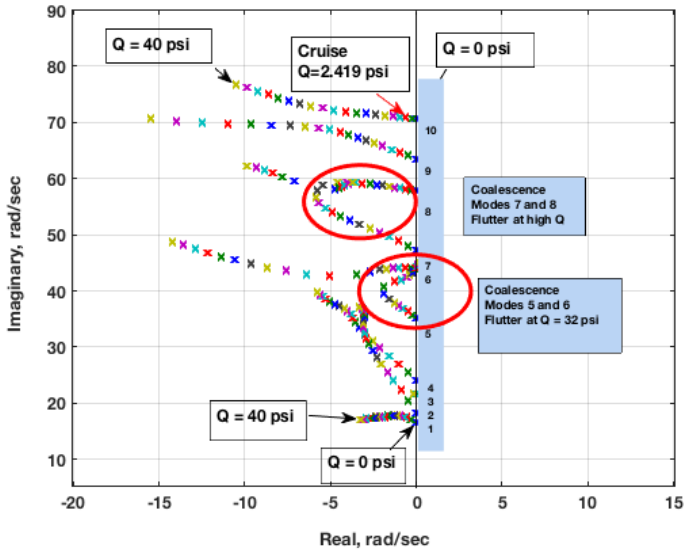

Figure 8: Aeroelastic root locus plot for the low-boom N+2 configuration at M=1.7 with each colored marker indicating a different dynamic pressure for a given mode.

4.2 KTH Generic Fighter

In 1985 and 1986, two wind-tunnel models of the Saab JAS 39 Gripen were designed, built, and tested in the NASA Transonic Dynamics Tunnel (TDT) for flutter clearance. One model, referred to as the stability model, was designed to be stiff, but incorporated proper scaling of both the mass and geometry. The other model, referred to as the flutter model, was also designed for proper scaling of structural dynamics, and was used for flutter testing with various external stores attached.

For the current collaboration, a generic fighter flutter-model version of these earlier models was selected. The new model, shown in Figure 9, has a similar outer mold line (OML) to the Gripen, but it has been modified into a more generic fighter configuration. Specifically, the air intakes were removed from the fuselage and the wing received an aspect ratio increase and a leading-edge sweep reduction. Details regarding the design, fabrication, and instrumentation of the wind-tunnel model can be found in the reference paper [33]. Figure 10 shows the wind-tunnel model installed in the TDT.

Using the AEROM software, aeroelastic root locus plots were generated for the KTH wind-

Figure 9: The generic fighter aeroelastic wind-tunnel model tested in summer of 2016.

Figure 10: The generic fighter aeroelastic wind-tunnel model installed in the Transonic Dynamics Tunnel (TDT).

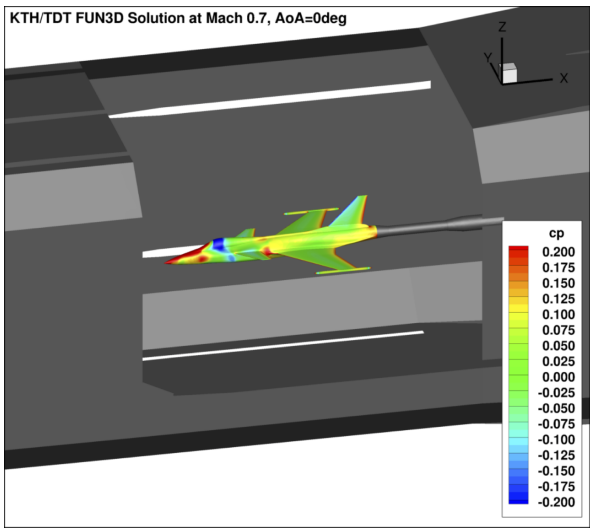

Figure 11: Pressure distributions at M=0.7, AoA=0 degrees on the wind-tunnel model, as simulated inside the TDT using FUN3D code.

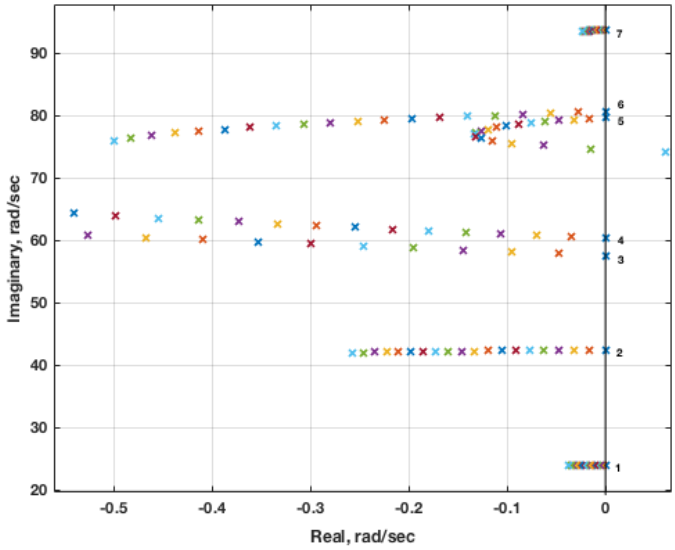

Figure 12: Root locus plot generated from ROM model indicating an aeroelastic instability at M=0.90 in air test medium for the third configuration.

tunnel model in air test medium for a free-air case and a solution accounting for the effects of the TDT test section via CFD modeling [34, 35], as can be seen in Figure 11. There were three configurations tested: wing with tip stores (configuration 1), wing with tip and under-wing stores (configuration 1), and wing with tip and under-wing stores with added masses at tip stores (configuration 3). The third configuration exhibited flutter while configurations 1 and 2 did not. Presented in Figure 12 is the aeroelastic ROM root locus plot for the free-air configuration at M=0.90. For this case, the roots clearly indicate a flutter mechanism at about 8100 N/m^2 (or 169 psf) via a coalescence of modes 5 and 6. Using the ROM, any dynamic pressure can be quickly evaluated to determine the aeroelastic response, consistent with the root locus plots. At this dynamic pressure, this result is above the experimental result at M=0.9 (not conservative). All results presented are for zero structural damping. Using the ROM, the effect of structural damping can be quickly evaluated as well but is not pursued in the present discussion.

Presented in Figures 13 and 14 are comparisons of the aeroelastic responses for modes 3, 4, 5, and 6 at M=0.9 and Q=7344 Pa for the FUN3D solution that includes the effect of the TDT and the ROM solution for the same configuration. As can be seen, the comparison is quite good with some variation in mode 6. Additional studies are currently underway to minimize these variations in order to reduce the error associated with the ROM.

For the CFD model that included the TDT, the ROM solution required two days whereas the full solution (for only one dynamic pressure) required five days. The ROM solution could, of course, then be used to rapidly compute the aeroelastic response due to any dynamic pressure.

4.3 AGARD 445.6 Wing

In this section, aeroelastic transients for the FUN3D full solution and aeroelastic transients and root locus plots are presented for the ROM results for both inviscid and viscous solutions of the AGARD 445.6 aeroelastic wing [36]. The FUN3D full solution results consist of aeroelastic transients at various dynamic pressures for two Mach numbers: M=0.96 and M=1.141. The

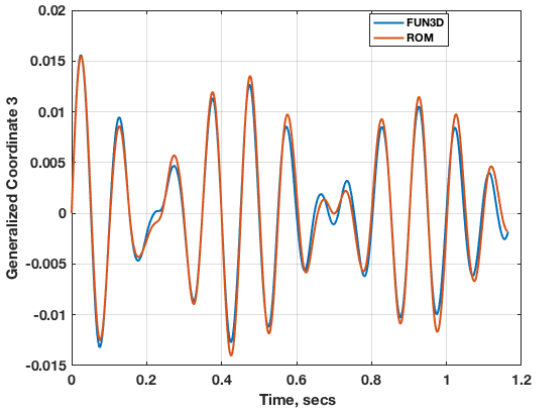

Figure 13: Aeroelastic response in mode 3 for the FUN3D and ROM solutions for the configuration including the TDT.

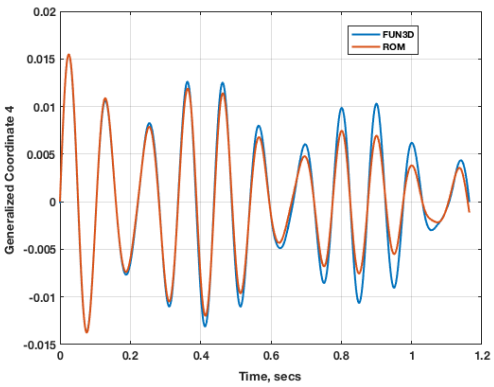

Figure 14: Aeroelastic response in mode 4 for the FUN3D and ROM solutions for the configuration including the TDT.

ROM results will consist of aeroelastic root locus plots for the same Mach numbers. The root locus plots generated using the ROM procedure described above are used to identify aeroelastic behavior and flutter mechanisms. The aeroelastic transients generated using the FUN3D full solutions are used to validate the ROM results at specific dynamic pressures.

4.3.1 Inviscid Results

In this section, inviscid FUN3D results are presented for both full FUN3D and ROM solutions. Presented in Figure 15 is the aeroelastic root locus plot for M=0.96 generated using the ROM method. These root locus plots contain root values at twenty dynamic pressures from zero to 114 psf. The reason for this increased resolution in dynamic pressure values is the ROM procedure itself. Because the ROM procedure generates a combined aeroelastic state-space model that consists of a state-space model of the structural dynamics and a state-space model of the unsteady aerodynamics (from FUN3D), root locus plots can be generated for any number and any increment of dynamic pressure in a matter of seconds. The flutter mechanism for the FUN3D inviscid solution at this Mach number is clearly dominated by the first mode with some coupling with the second mode noticeable. The third and fourth modes are stable.

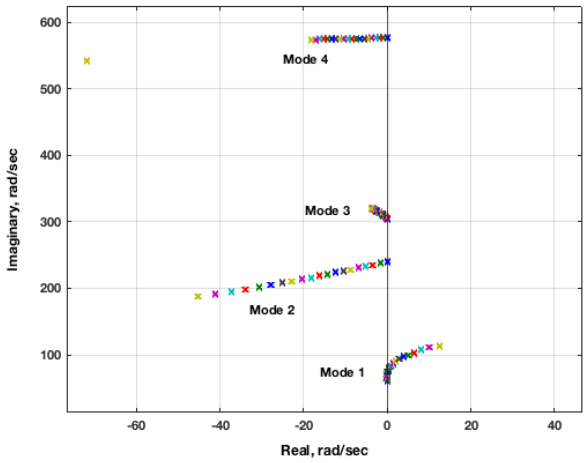

Figure 15: ROM aeroelastic root locus plot for M=0.96, inviscid solution.

In order to better visualize the root migrations for the first mode, a zoomed-in version of the root locus plot is presented as Figure 16. The increment in dynamic pressure for this root locus plot is 6 psf starting with 0 psf yielding a flutter dynamic pressure of approximately 30 psf. The flutter dynamic pressure is, therefore, about 30 psf. This result is very close to and consistent with the FUN3D full solution flutter dynamic pressure presented in the references [36]. However, the inviscid result at this Mach number does not compare well with the experiment. This discrepancy is not surprising as inviscid solutions tend to have stronger shocks that are farther aft and therefore induce a stronger and earlier onset of flutter. When viscosity is introduced into the solution, the shock strength is reduced and the shock position is moved forward resulting in the onset of flutter at a higher dynamic pressure. This effect is discussed in the next section of this paper.

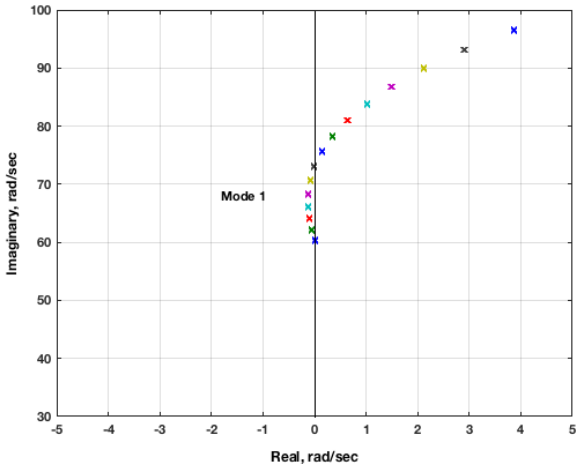

Figure 16: Detailed view of ROM aeroelastic root locus plot for M=0.96, inviscid solution.

Solutions are now presented for the supersonic Mach number of 1.141. As presented in the references [36], there is a wide variation of flutter dynamic pressures and flutter frequencies at this condition. The discrepancy between many of the solutions and the experiment as well as

the discrepancy amongst the various solution methods has long been a source of speculation. Although the authors do not present a conclusive answer to the source of these discrepancies, it is hoped that the results presented will spur additional discussion and research.

Figure 17 presents the aeroelastic root locus plot for M=1.141 generated using the FUN3D ROM method. There are two obvious flutter mechanisms: one flutter mechanism is an instability involving the first mode while the other flutter mechanism involves an instability of the third mode. The third mode is always unstable while the first mode instability occurs at a dynamic pressure of about 300 psf. The third mode instability was a surprise in that it is not mentioned by other researchers. So in order to validate the accuracy of this aeroelastic root locus plot, the generalized coordinates from a FUN3D full solution are inspected.

Presented in Figure 18 are the aeroelastic transients for the four modes at M=1.141 and a dynamic pressure of 30 psf. The first mode, with the largest amplitude, is clearly stable. However, discerning the stability for the other three modes with smaller and similar amplitudes is not as obvious as it is for the first mode. If only the third mode is visualized, as in Figure 19, the unstable nature of this mode becomes clearer.

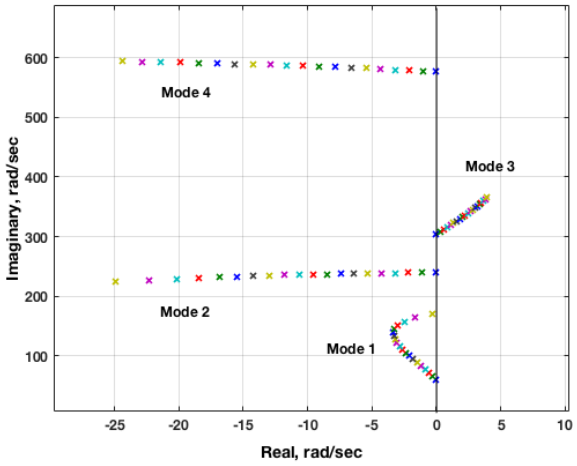

Figure 17: ROM aeroelastic root locus plot for M=1.141, inviscid solution.

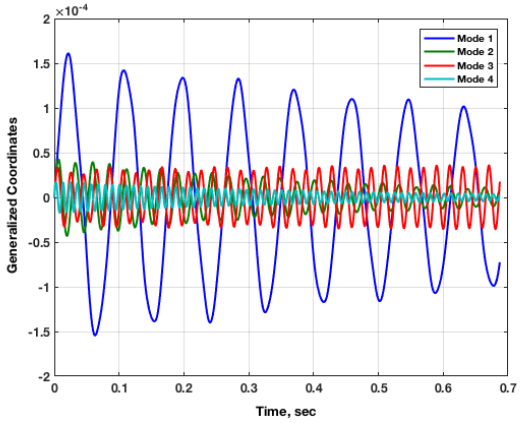

Figure 18: FUN3D full solution generalized coordinates at M=1.141, Q=30 psf, inviscid solution.

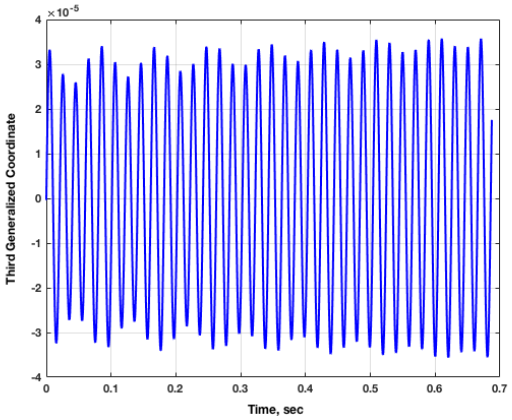

Figure 19: FUN3D full solution third generalized coordinate at M=1.141, Q=30 psf, inviscid solution.

This third mode instability, not mentioned in any other publications on the flutter boundary of the AGARD 445.6 wing, raises an important question. Is this third mode instability present in all inviscid (Euler) solutions of the AGARD 445.6 wing presented in the literature? The answer to this question requires consultation with researchers that have performed inviscid CFD aeroelastic analyses for this wing at this condition. However, as mentioned previously, it appears that the focus of all previous inviscid analyses at supersonic conditions was the first mode instability. If that is the case, it is easy to see how the third mode instability might have been ignored. In addition, for analyses performed in the early days of computational aeroelasticity, Figure 18 would have consisted of fewer time steps (due to computational cost at the time), thereby making it difficult to visually notice the third mode instability. It should be stated that the authors have confirmed the existence of this third mode instability in previous solutions obtained using the CFL3D code.

4.3.2 Viscous Results

In this section, viscous FUN3D full and ROM solutions are presented at M=1.141 since significant discrepancies, as just discussed, exist at this condition. The results for FUN3D full and ROM solutions at subsonic Mach numbers agree well with each other and with experiment and are not presented in this paper.

Presented in Figure 20 is the root locus plot generated using the FUN3D ROM viscous solution at M=1.141 in dynamic pressure increments of 6 psf to 114 psf. It appears that the third mode instability exhibited by the inviscid solution has been stabilized by the inclusion of viscous effects.

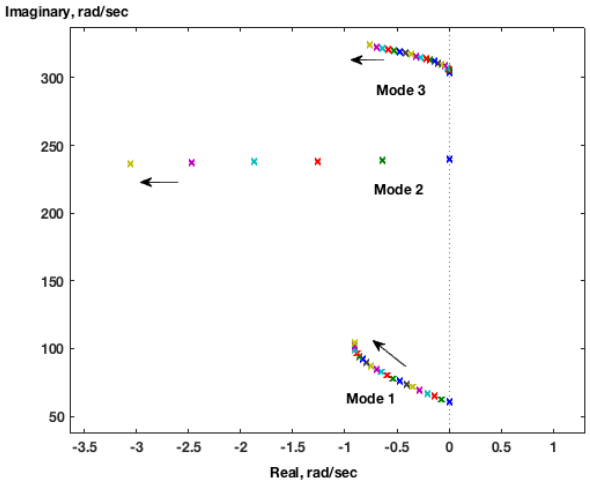

Figure 20: Viscous ROM root locus plot at M=1.141.

The four generalized coordinates from a FUN3D full viscous solution are presented as Figure 21. At this low dynamic pressure, all four generalized coordinates are minimally damped. Visual analysis of these generalized coordinates indicates that these generalized coordinates appear to be stable although minimally damped. However, it is important to state a fundamental and important difference between a root locus plot and the visual, or otherwise post-processed analysis of generalized coordinates over a short period of time. A root locus plot, by definition, exhibits the roots of a system as time approaches infinity or as the system reaches steady state. In contrast, the analysis of the initial transient response of a generalized coordinate over a short period of time can be deceiving as the response can change if the response was viewed (or analyzed) over a longer period of time. This property of root locus plots is critical for the accurate evaluation of aeroelastic stability.

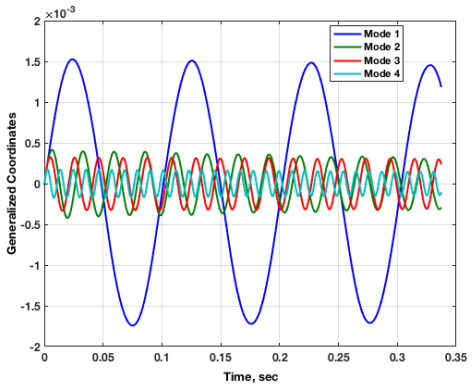

Figure 21: Generalized coordinates from viscous FUN3D full solution at M=1.141 and Q=6 psf.

5 CONCLUDING REMARKS

The origin, implementation, and applications of AEROM, the patented NASA reduced-order modeling software, have been presented. Recent applications of the software to analyze complex configurations, including computation of the aeroelastic responses of the Lockheed-Martin low-boom N+2 configuration, the KTH (Royal Institute of Technology, Sweden) generic fighter

wind-tunnel model, and the AGARD 445.6 wing were presented. Results presented demonstrate the computational efficiency and analytical capability of the AEROM software.

COPYRIGHT STATEMENT

6 REFERENCES

[1] Adams, W. M. and Hoadley, S. T., "ISAC: A Tool for Aeroservoelastic Modeling and Analysis," *Proceedings of the 34th AIAA/ASME/ASCE/AHS/ASC Structures, Structural Dynamics, and Materials Conference*, La Jolla, CA, April 1993, AIAA-1993-1421.

[2] Silva, W. A., "Simultaneous Excitation of Multiple-Input/Multiple-Output CFD-Based Unsteady Aerodynamic Systems," *Journal of Aircraft*, Vol. 45, No. 4, July-August 2008, pp. 1267–1274.

[3] Silva, W. A., Vatsa, V. N., and Biedron, R. T., "Development of Unsteady Aerodynamic and Aeroelastic Reduced-Order Models Using the FUN3D Code," IFASD Paper No. 2009-30, presented at the International Forum on Aeroelasticity and Structural Dynamics, Seattle, WA, June 2009.

[4] Silva, W. A., Vatsa, V. N., and Biedron, R. T., "Reduced-Order Models for the Aeroelastic Analyses of the Ares Vehicles," AIAA Paper No. 2010-4375, presented at the 28th AIAA Applied Aerodynamics Conference, Chicago, IL.

[5] Silva, W. A., *Discrete-Time Linear and Nonlinear Aerodynamic Impulse Responses for Efficient CFD Analyses*, Ph.D. thesis, College of William & Mary, December 1997.

[6] Silva, W. A., "Identification of Linear and Nonlinear Aerodynamic Impulse Responses Using Digital Filter Techniques," AIAA Paper 97-3712, August 1997.

[7] Silva, W. A., "Reduced-Order Models Based on Linear and Nonlinear Aerodynamic Impulse Responses," *CEAS/AIAA/ICASE/NASA Langley International Forum on Aeroelasticity and Structural Dynamics, Williamsburg, VA*, June 1999, pp. 369–379.

[8] Juang, J.-N. and Pappa, R. S., "An Eigensystem Realization Algorithm for Modal Parameter Identification and Model Reduction," *Journal of Guidance, Control, and Dynamics*, Vol. 8, 1985, pp. 620–627.

[9] Juang, J.-N., *Applied System Identification*, Prentice-Hall PTR, 1994.

[10] Silva, W. A. and Raveh, D. E., "Development of Unsteady Aerodynamic State-Space Models from CFD-Based Pulse Responses," AIAA Paper No. 2001-1213, presented at the 42nd Structures, Structural Dynamics, and Materials Conference, Seattle, WA.

[11] Gaitonde, A. L. and Jones, D. P., "Study of Linear Response Identification Techniques and Reduced-Order Model Generation for a 2D CFD Scheme," *Journal for Numerical Methods in Fluids*, Vol. 52, 2006, pp. 1367–1402.

[12] Gaitonde, A. L. and Jones, D. P., "Calculations with ERA Based Reduced-Order Aerodynamic Models," *24th Applied Aerodynamics Conference*, No. 2006, San Francisco, CA, June 2006.

[13] Griffiths, L., Jones, D. P., and Friswell, M. I., "Model Updating of Dynamically Time Linear Reduced-Order Models," *International Forum on Aeroelasticity and Structural Dynamics*, No. 2011, Paris, France, June 2011.

[14] Fleischer, D. and Breitsamter, C., "Efficient Computation of Unsteady Aerodynamic Loads Using Computational Fluid Dynamics Linearized Methods," *Journal of Aircraft*, Vol. 50, 2013, pp. 425–440.

[15] Xiaoyan, L., Zhigang, W., and Chao, Y., "Aerodynamic Reduced-Order Models Based on Observer Techniques," *51st AIAA/ASME/ASCE/AHS/ASC Structures, Structural Dynamics, and Materials Conference*, No. 2010, Orlando, FL, April 2010.

[16] Song, H., Qian, J., Wang, Y., Pant, K., Chin, A. W., and Brenner, M. J., "Development of Aeroelastic and Aeroservoelastic Reduced-Order Models for Active Structural Control," *56th AIAA/ASCE/AHS/ASC Structures, Structural Dynamics, and Materials Conference*, No. 2015, Kissimmee, FL, Jan 2015.

[17] Ma, Z., Ahuja, S., and Rowley, C. W., "Reduced-Order Models for Control of Fluid Using the Eigensystem Realization Algorithm," *Theoretical Computational Fluid Dynamics*, Vol. 25, 2011, pp. 233–247.

[18] Silva, W. A. and Bartels, R. E., "Development of Reduced-Order Models for Aeroelastic Analysis and Flutter Prediction Using the CFL3Dv6.0 Code," *Journal of Fluids and Structures*, No. 19, 2004, pp. 729–745.

[19] Krist, S. L., Biedron, R. T., and Rumsey, C. L., "CFL3D User's Manual Version 5.0," Tech. rep., NASA Langley Research Center, 1997.

[20] Kim, T., Hong, M., Bhatia, K. G., and SenGupta, G., "Aeroelastic Model Reduction for Affordable Computational Fluid Dynamics-Based Flutter Analysis," *AIAA Journal*, Vol. 43, 2005, pp. 2487–2495.

[21] Silva, W. A., "Recent Enhancements to the Development of CFD-Based Aeroelastic Reduced Order Models," *48th AIAA/ASME/ASCE/AHS/ASC Structures, Structural Dynamics, and Materials Conference*, No. AIAA Paper No. 2007-2051, Honolulu, HI, April 23-26 2007.

[22] Anderson, W. K. and Bonhaus, D. L., "An Implicit Upwind Algorithm for Computing Turbulent Flows on Unstructured Grids," *Computers and Fluids*, Vol. 23, No. 1, 1994, pp. 1–21.

[23] NASA LaRC, Hampton, VA, *FUN3D Manual, v12.9*, Nov. 2015, http://fun3d.larc.nasa.gov.

[24] Biedron, R. T., Vatsa, V. N., and Atkins, H. L., "Simulation of Unsteady Flows Using an Unstructured Navier-Stokes Solver on Moving and Stationary Grids," AIAA Paper 2005-5093, 2005.

[25] Biedron, R. T. and Thomas, J. L., "Recent Enhancements to the FUN3D Flow Solver for Moving-Mesh Applications," AIAA Paper 2009-1360, Jan.

[26] Samareh, J., "Discrete Data Transfer Technique for Fluid-Structure Interaction," *18th AIAA Computational Fluid Dynamics Conference*, No. 2007, Miami, FL, Jun 2007.

[27] Juang, J.-N., Phan, M., Horta, L. G., and Longman, R. W., "Identification of Observer/Kalman Filter Markov Parameters: Theory and Experiments," *Journal of Guidance, Control, and Dynamics*, Vol. 16, 1993, pp. 320–329.

[28] Eykhoff, P., *System Identification: Parameter and State Identification*, Wiley Publishers, 1974.

[29] Ljung, L., *System Identification: Theory for the User*, Prentice-Hall Publishers, 1999.

[30] Zhu, Y., *Multivariable System Identification for Process Control*, Pergamon Publishers, 2001.

[31] Pacheco, R. P. and V. Steffen, J., "Using Orthogonal Functions for Identification and Sensitivity Analysis of Mechanical Systems," *Journal of Vibration and Control*, Vol. 8, June 2002, pp. 993–1021.

[32] Raveh, D. E., "Identification of Computational-Fluid-Dynamic Based Unsteady Aerodynamic Models for Aeroelastic Analysis," *Journal of Aircraft*, Vol. 41, June 2004, pp. 620–632.

[33] Silva, W. A., Ringertz, U., Stenfelt, G., Eller, D., Keller, D. F., and Chwalowski, P., "Status of the KTH Wind-Tunnel Test for Acquisition of Transonic Nonlinear Aeroelastic Data," *AIAA SciTech, 15th Dynamics Specialists' Conference*, No. AIAA paper 2016-2050, Jan. 2016.

[34] Silva, W. A., Chwalowski, P., Wieseman, C. D., Keller, D. F., Eller, D., and Ringertz, U., "Computational and Experimental Results for the KTH-NASA Wind-Tunnel Model Used for Acquisition of Transonic Nonlinear Aeroelastic Data," *International Forum on Aeroelasticity and Structural Dynamics, 2017*, No. IFASD paper 181, June 2017.

[35] Chwalowski, P., Silva, W. A., Wieseman, C. D., and Heeg, J., "CFD Model of the Transonic Dynamics Tunnel with Applications," *International Forum on Aeroelasticity and Structural Dynamics, 2017*, No. IFASD paper 44, June 2017.

[36] Silva, W. A., Chwalowski, P., and Perry, B., "Evaluation of Linear, Inviscid, Viscous, and Reduced-Order Modeling Aeroelastic Solutions of the AGARD 445.6 Wing Using Root Locus Analysis," *International Journal of Computational Fluid Dynamics*, Vol. 28, 2014.